Journal of Power Sources 206 (2012) 70–76

Contents lists available at SciVerse ScienceDirect

Journal of Power Sources

journal homepage: www.elsevier.com/locate/jpowsour

Sandvik Sanergy HT – A potential interconnect material for $LaNbO_4$-based proton ceramic fuel cells

Anders Werner Bredvei Skilbred, Reidar Haugsrud*

Department of Chemistry, Centre for Materials Science and Nanotechnology, University of Oslo, FERMiO, Gaustadalleen 21, NO-0349 Oslo, Norway

ARTICLE INFO

Article history:
Received 7 September 2011
Received in revised form 13 January 2012
Accepted 15 January 2012
Available online 23 January 2012

Keywords:
Proton ceramic fuel cell
Interconnect
Sandvik Sanergy HT
Oxidation kinetics
Thermal expansion
Area specific resistance

ABSTRACT

High temperature properties of Sandvik Sanergy HT have been studied to evaluate the alloy's suitability as an interconnect material for $LaNbO_4$ based proton ceramic fuel cells (PCFCs). The thermal expansion behavior of the alloy deviates from $LaNbO_4$ at higher temperatures which may be unfavorable, however the average values for the two materials over the whole temperature region are rather similar. The oxidation kinetics was parabolic and the rate constants were low at temperatures below 1000 °C. Accelerated oxidation was encountered after 300 h at 1000 °C revealing that the material may undergo severe degradation at sufficiently high temperatures. A complex oxide scale containing an inner layer of chromium oxide and an outer layer of various spinel phases containing chromium, manganese and iron was formed at all temperatures. As a consequence of high oxidation resistance and an oxide with relatively high electronic conductivity, the area specific resistance (ASR) of Sandvik Sanergy HT measured at 700 °C proved to be low.

1. Introduction

High temperature proton ceramic fuel cells (PCFCs) are promising for future clean energy conversion systems [1,2]. PCFCs have the advantage of potentially high fuel efficiencies and diverse fuel utilization. In principle one may apply reduced operating temperatures (600–700 °C) compared to YSZ-based solid oxide fuel cells (SOFCs) (750–900 °C) which facilitates less complex and costly materials in the assembly, in particular for the interconnect material. Acceptor doped lanthanum niobate (e.g. $La_{0.995}Ca_{0.005}NbO_4$) is one of the high temperature ceramic proton conductors currently under investigation as electrolyte in PCFCs [1,3]. With its good chemical stability this material is an interesting electrolyte alternative, although the proton conductivity is more than one order of magnitude lower than for the chemically less stable alkaline earth based perovskite structured cerates.

With a new electrolyte material the entire fuel cell assembly has to be adapted, including the interconnect material. The main purpose of the interconnect is to provide electrical contact between the anode and cathode, besides separating the fuel and the air. This requires a gas tight material with high electronic conductivity and mechanical strength, even after long term high temperature operation facing oxidizing and reducing atmospheres.

Some ferritic stainless steels are regarded as the best candidates for metallic interconnects in SOFCs [4–6]. This is due to the relatively high oxidation resistance and formation of electrically conducting oxide scales, combined with acceptable thermal expansion compatibility. Sandvik Sanergy HT is a relatively new stainless steel developed specifically to meet the requirements of SOFC interconnects [7,8]. The aim of this study was to investigate further the high temperature properties of the Sandvik Sanergy HT alloy, including thermal expansion behavior, the oxidation mechanism and the area specific resistance (ASR) of oxide scales. Based on the results the material's applicability as interconnect for $LaNbO_4$-based PCFCs was evaluated.

2. Experimental

The Sandvik Sanergy HT alloy, with composition as listed in Table 1, was cut into samples of dimension ~20 mm × 15 mm × 0.5 mm and ground with SiC paper grade 1200 before being ultrasonically cleaned for 10 min in ethanol.

Thermal expansion behavior was determined in the temperature range 25–1000 °C in dry nitrogen atmosphere using a Netzsch DIL 402C.

The oxidation behavior was monitored with a CI Robal MK1 microbalance attached to a vertical resistance heated tube furnace, under constant flow (0.45 l h^{-1}) of either wet (~2.5% H_2O) or dry (~30 ppm H_2O) air at temperatures of 700, 800, 850, 900 and 1000 °C. The samples were suspended into the hot zone of the furnace at the respective exposure temperature, and after

* Corresponding author. Tel.: +47 22840659; fax: +47 22840651.
E-mail address: reidar.haugsrud@smn.uio.no (R. Haugsrud).

0378-7753/$ – see front matter © 2012 Elsevier B.V. All rights reserved.
doi:10.1016/j.jpowsour.2012.01.101

Table 1
Chemical composition, wt. %, of Sandvik Sanergy HT [8].

Cr	Mn	Si	C	Mo	Nb	Add.	Fe
22	≤0.5	≤0.30	≤0.05	1.0	0.75	Ti	Bal.

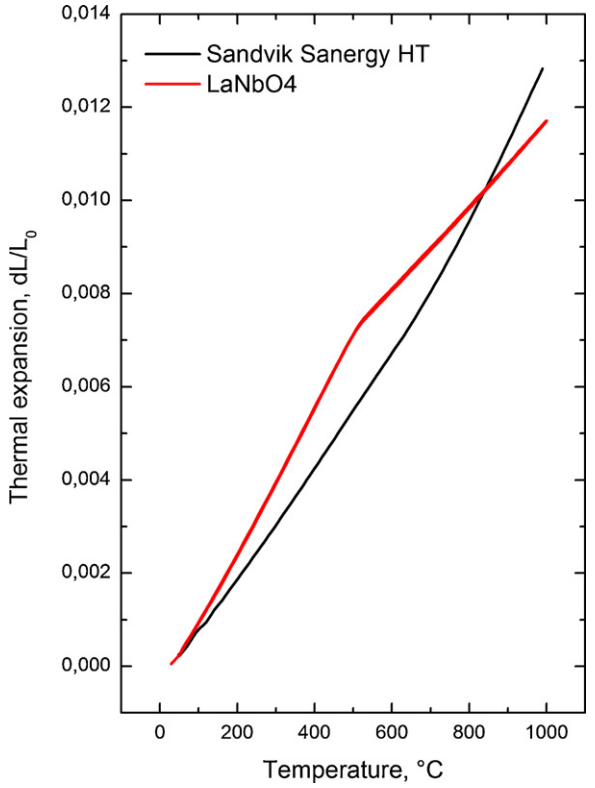

Fig. 1. Thermal expansion behavior of Sandvik Sanergy HT compared to $LaNbO_4$, a candidate electrolyte material for PCFCs.

oxidation, the samples were retracted from the furnace and air cooled.

For ASR measurements two samples were pre-oxidized for 24 h at 700 °C in wet air, and two gold wires were spot welded on each sample for contacting purposes. The samples were then sandwiched together with a contact layer of Pt ink and Pt grid

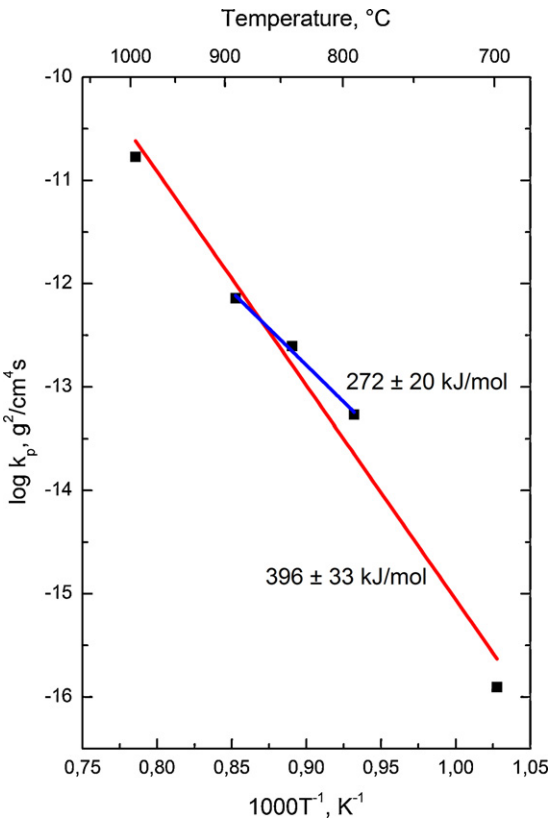

Fig. 3. Parabolic rate constants plotted as a function of inverse temperature. The graph also includes calculated activation energies of oxidation representing the two slopes.

in a ProboStat (NorECs AS) measurement cell. The assembly was held together with a spring load. A constant current was applied and the resulting voltage drop over the interface between the two samples was measured using an Agilent 35210 data acquisition unit with a voltmeter switch module. Contributions to the resistivity from the alloy itself and the platinum contact layer were considered negligible. The setup was tested for several currents and the resulting voltage behaved according to Ohm's law.

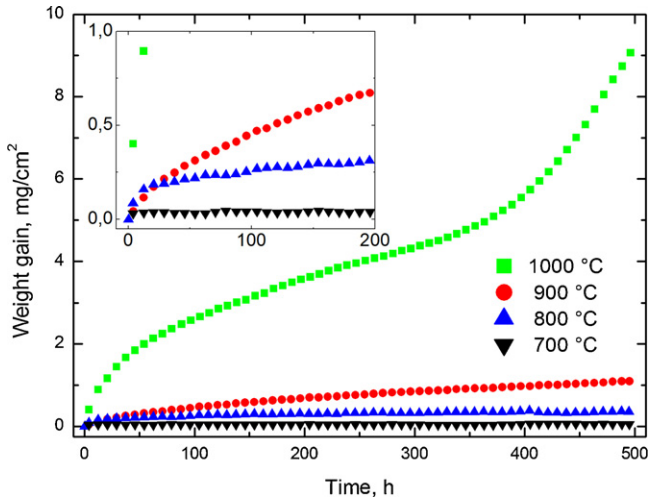

Fig. 2. Oxygen uptake recorded during oxidation of Sandvik Sanergy HT at various temperatures in wet air.

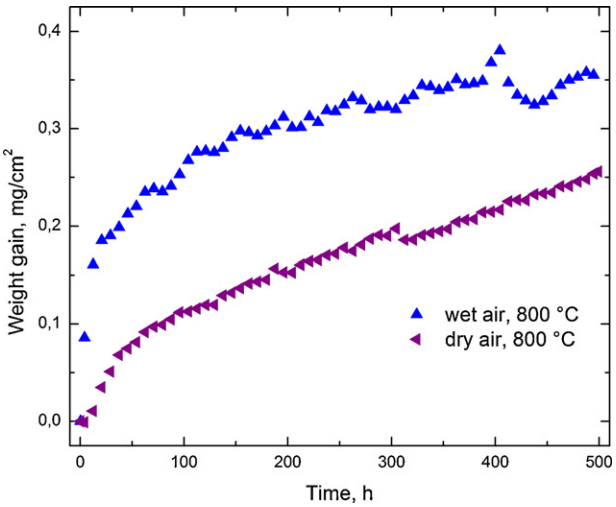

Fig. 4. Oxygen uptake of Sandvik Sanergy HT measured by thermogravimetry at 800 °C in wet and dry air atmosphere.

The microstructure and composition of the oxide scale and the alloy were characterized after the experiments by means of a FEI Quanta 200F scanning electron microscope (SEM) equipped with an energy dispersive spectrometer (EDS) and operated with an acceleration voltage of 20 kV. In order to assess the phase composition in the oxide scales, X-ray diffraction (XRD) was carried out using a Siemens D5000 with CuKα_1 radiation (45 kV, 40 mA).

3. Results

As we saw in the previous section, experimental approaches were utilized in this study to characterize the Sandvik Sanergy HT with respect to the thermal expansion behavior, area specific resistance and the corrosion resistance – essential material properties for an interconnect candidate material.

3.1. Thermal expansion

The thermal expansion behavior of the Sandvik Sanergy HT and $LaNbO_4$ from room temperature up to 1000 °C is displayed in Fig. 1. The average linear thermal expansion coefficient (TEC) for the alloy over the whole temperature interval is 12.9×10^{-6} °C^{-1}. As for most iron-based alloys the slope of the curve increases steadily, revealing that the TEC gradually increases with increasing temperature. For $LaNbO_4$, a break in the curve is encountered at ~510 °C as a consequence of the phase transformation from the monoclinic low temperature phase to the tetragonal high temperature phase [9,10]. Comparing the two materials there are large differences in TEC values for both the low and the high temperature region, meanwhile the average values across the whole temperature window are rather similar (cf. Table 2).

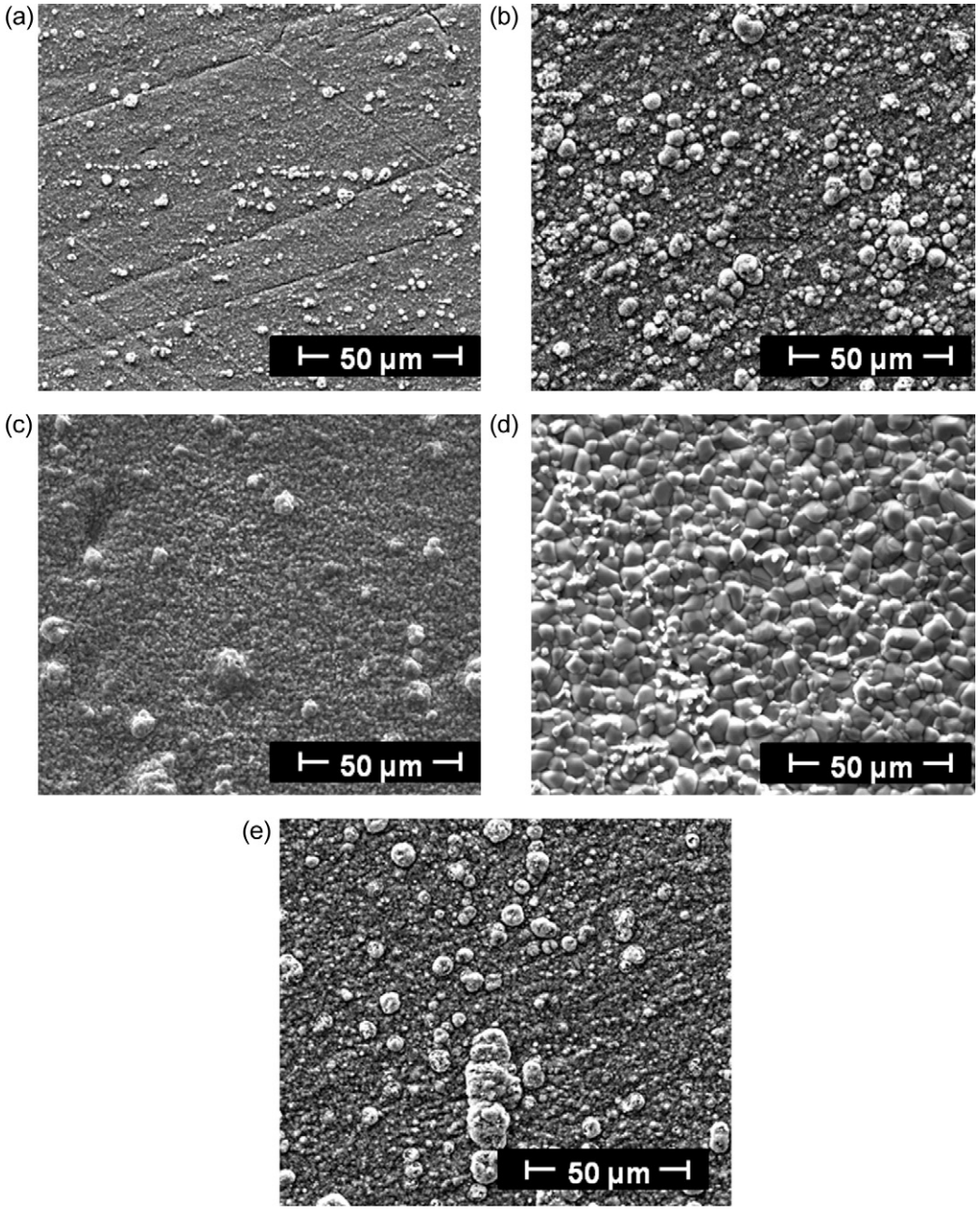

Fig. 5. Secondary electron SEM surface images of Sandvik Sanergy HT oxidized for 500 h in wet air atmosphere at (a) 700 °C, (b) 800 °C, (c) 900 °C and (d) 1000 °C, and (e) dry air at 800 °C.

Table 2
Thermal expansion coefficients (TECs) for Sandvik Sanergy HT and $LaNbO_4$ at different temperature intervals.

Thermal expansion coefficients (TEC)		
Temperature	Sanergy HT	$LaNbO_4$
100–510 °C	11.7×10^{-6} °C^{-1}	15.4×10^{-6} °C^{-1}
550–900 °C	14.5×10^{-6} °C^{-1}	8.9×10^{-6} °C^{-1}
100–900 °C	12.9×10^{-6} °C^{-1}	12.3×10^{-6} °C^{-1}

3.2. Thermogravimetry

Fig. 2 presents the weight change of the alloy as a function of time during exposure to wet air at 700, 800, 900 and 1000 °C as measured by thermogravimetry. At 700 °C the oxidation rate was low; a weight gain of only ~0.05 mg cm^{-2} was observed over 500 h. At 800 and 900 °C, parabolic kinetics is encountered throughout the duration of the experiment. The oxidation behavior at 1000 °C corresponds to a similar parabolic behavior during the first 300 h after which the oxidation accelerates. An Arrhenius representation of the parabolic rate constants, k_p, is shown in Fig. 3. Based on the temperature dependence of k_p the activation energy, E_a, for the oxidation over the whole temperature range was calculated to be 396 ± 33 kJ mol^{-1}. This value is higher than normally reported for the formation of oxide scales on chromia forming iron based alloys [11,12]. However, the calculated activation energy in the temperature range from 800 to 900 °C was 272 ± 20 kJ mol^{-1}, which correspond to typical literature values (approx. 250 kJ mol^{-1}) for similar alloys [11–14].

Fig. 4 presents the recorded weight change due to oxidation in wet and dry air at 800 °C as a function of time. The oxidation rate is initially higher under humidified conditions followed by similar kinetic behavior as under dry conditions.

3.3. Surface characterization

Fig. 5 presents SEM observations of samples oxidized in wet and dry air for 500 h at various temperatures. The surface morphology consisted of small cubes and larger nodules randomly distributed over the surface. The average oxide particle size increases with temperature from ~0.2 μm at 700 °C to ~3.9 μm at 1000 °C. The figures also compare the surface morphologies of the samples oxidized at 800 °C in dry (Fig. 5e) and wet air (Fig. 5b), indicating a more extensive formation of nodules under wet conditions.

From EDS investigations of the surface it became clear that the overall composition varied with the reaction temperature. The iron signal, which reflects contribution from the alloy substrate, decreased with temperature as a result of thicker oxide scales. One exception from this was the sample oxidized at 1000 °C for 500 h, where the iron signal was significantly higher compared to the samples exposed to 800 °C and 900 °C. The chromium content in the surface goes through a maximum for the samples oxidized at 800 °C and 900 °C, meanwhile the level of manganese increases steadily with increasing oxidation temperature. At 1000 °C, manganese was the dominating cation at the surface followed by chromium. When comparing samples oxidized in dry and wet air at 800 °C, it is seen that dry atmospheres yield a surface slightly richer in iron.

The most prominent oxide phases for the different temperatures identified by XRD were Cr_2O_3 and (Cr, Mn, Fe)$_3O_4$ spinels (Fig. 6), which correspond well to the elemental composition from EDS. However, the exact composition of the spinel phases was difficult to establish.

3.4. Cross sectional analysis

Cross sections of all samples were investigated using SEM and EDS line scan, and the images in Fig. 7 show samples, oxidized for

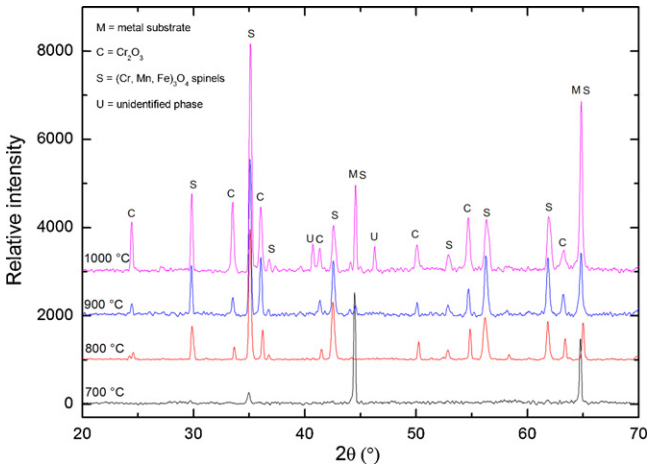

Fig. 6. XRD patterns of Sandvik Sanergy HT after 500 h of oxidation in wet air at 700, 800, 900 and 1000 °C.

500 h at various temperatures from 700 °C to 1000 °C. The figures also include EDS line scans illustrating the distribution of Fe, Cr, Mn and O in the alloy and throughout the oxide scale.

The oxide scale formed at 700 °C was thin (cf. Fig. 7a), and its thickness and uniformity could not be determined accurately by SEM. However, line scan shows a significant peak in the Cr and Mn signal at the outer surface of the sample accompanied by a sharp fall in the Fe signal. The limited oxide thickness may allow the underlying alloy to strongly influence both surface EDS and XRD signal.

At 800 °C the oxide scale formed in wet and dry air was continuous and dense with similar thicknesses of ~1.3 μm (Fig. 7b) and ~1.5 μm (cf. Fig. 7e) respectively. Thermogravimetry, conversely, shows that dry conditions resulted in lower weight gain (cf. Fig. 4) which may indicate a slightly more porous oxide layer. The EDS line scans showed for both samples that the inner region of the oxide scale was rich in Cr, while in the outer part the amount of Mn increases towards the oxide–gas interface. This observation is in accordance with the surface EDS and XRD from which Cr_2O_3 and (Cr, Mn, Fe)$_3O_4$ spinel phases were identified.

The oxides formed on the samples oxidized at 900 °C and 1000 °C in wet air were dense and continuous (cf. Fig. 7c and d) with thicknesses of ~6 μm and ~28 μm, respectively. From the contrast in the backscatter image, the oxide layer appeared to consist of two different regions. EDS line scans showed again a Cr rich inner oxide layer while only a small fraction of the outer part of the scale contained any significant amounts of Mn.

For all temperatures, pores were observed in the outer part of the alloy (up to ~20 μm depth). The size and number of these pores increased with increasing oxidation temperature.

Backscattered electron images of all the samples also showed some bright precipitates inside the alloy representing so called Laves phase, in particular close to the oxide–alloy interface. EDS analyses indicated that these areas contained mostly Nb and Mo.

3.5. Area specific resistance, ASR

Fig. 8 shows that the average ASR of the two forming oxide scales decreases as a function of time at 700 °C on the pre-oxidized samples. The decrease in ASR represents the gradually improved contact between the two sandwiched samples during the high temperature treatment. As seen from the figure, the ASR reaches a stable value of ~6 mΩ cm^2 after approximately 350 h.

4. Discussion

Thermogravimetry showed that the oxidation kinetics of Sandvik Sanergy HT was parabolic, and that the oxidation resistance is comparable to similar ferritic stainless steels, Table 3 [15–19]. The oxide scale consisted of a Cr_2O_3 layer close to the alloy–oxide interface while towards the oxide–gas interface the Mn content increased, revealing formation of $(Cr, Mn)_3O_4$ spinel phases.

Parabolic kinetics is generally an evidence of processes rate limited by diffusion, and high Cr and Mn contents in the outer part of the oxide indicate that the scales grow mainly by outward diffusion of cations. The oxide is relatively dense and adherent, limiting ingress of gaseous oxygen, and since the cation and oxide ion diffusivities in the oxides formed are low, the scale acts as an effective barrier towards extensive materials degradation. The level of Mn in the scale increases considerably with increasing temperature, and especially for the samples oxidized at 900 °C and 1000 °C the Mn content was pronounced. Accordingly, transport of Mn through the oxide scales may be substantial at high temperatures, as also expected from literature [20–23]. This could be a result of

Table 3
Parabolic rate constants, k_p, for various ferritic stainless interconnect alloys oxidized in air at 800 °C.

Alloy	$k_p(\times 10^{-14}\ g^2\ cm^{-4}\ s^{-1})$	Ref.
Sanergy HT	5.4	This study
ZMG 232	27	[15]
AL453	39	[17]
Crofer 22 APU	2.8–8.0	[15–17]
SUS 430	8.5	[18,19]

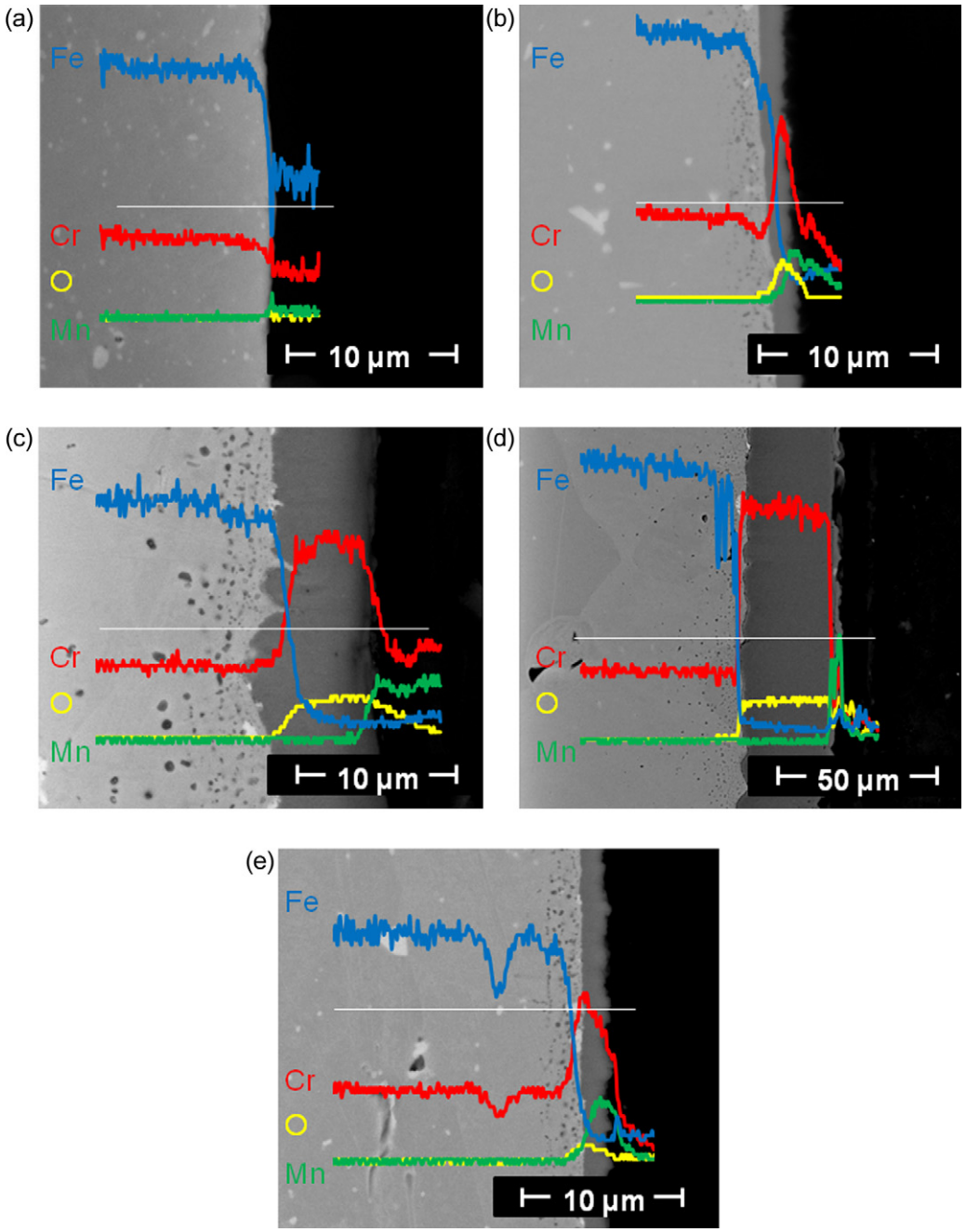

Fig. 7. Backscattered electron SEM image of cross sectioned Sandvik Sanergy HT oxidized for 500 h in wet air atmosphere at (a) 700 °C, (b) 800 °C, (c) 900 °C and (d) 1000 °C, and (e) in dry air at 800 °C. The figure also includes EDS line scans showing the elemental distribution of Fe, Cr, Mn and O.

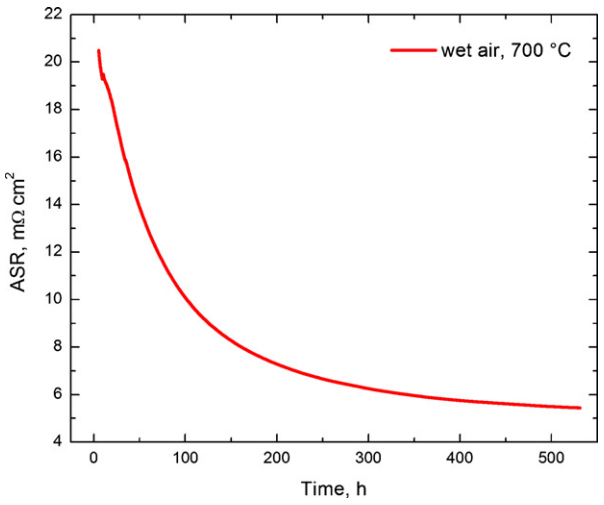

Fig. 8. Area specific resistance for Sandvik Sanergy HT with Pt contact layer, measured at 700 °C in wet air.

fast Mn diffusion, compared to the other major alloying elements, i.e. Cr and Fe, enabling the formation of Mn containing oxide phases at the outer surface [21]. However, others report that the diffusion coefficients of Mn and Cr are similar, and that MnO and Cr_2O_3 may alternatively form simultaneously during the initial stage of oxidation [22]. If both cations diffuse with approximately equal rates through the forming oxide, Mn is, due to its limited amount in the alloy, only present in the outer part of the scale.

The overall temperature dependence does not follow a straight-line Arrhenius behavior; the oxidation is more activated at low and high temperatures. On this basis one may speculate whether the same oxidation mechanism prevails from 700 °C to 1000 °C. Brylewski et al. attributed highly activated oxidation for a similar alloy in the lower temperature region from 750 to 825 °C to anion diffusion in chromia as a consequence of an oxidation process governed by the counter-current chromium and oxygen diffusion through Cr_2O_3 grain boundaries [13,24,25]. The activation energy for the oxidation process estimated from k_p between 800 °C and 900 °C is comparable to the activation energy reported for Cr diffusion in Cr_2O_3 and we, accordingly, consider outward diffusion of Cr to be the limiting step in the overall oxidation for this temperature region [11–13,26]. At 1000 °C accelerated oxidation is observed after ~300 h and since the composition of the scale differs somewhat compared to the lower temperatures this indicates a slightly different oxidation mechanism. Overall, these effects result in a non-linear Arrhenius behavior reflecting the complex situation in the scales with transport of several cations with different temperature dependences.

Thermogravimetry (Fig. 4) showed that the initial rate of oxidation is higher in wet than in dry atmosphere, as observed for many other alloys at high temperatures [24,27]. One may speculate whether the high initial rate is a result of faster dissociation of water compared to oxygen or that water effectively catalyzes oxygen dissociation yielding easier nucleation and initial growth under wet than dry conditions.

By dissolution of protons in the form of hydroxide species water containing atmospheres may modify the defect structure [28–30]. Chromium oxide is a p-type semi-conductor under oxidizing conditions chromium vacancies, the formation of hydroxide species may be charge compensated by metal vacancies [28,31–33]. Since the oxidation of chromia formers is dominated by outward cation transport via metal vacancies, dissolution of protons should, consequently, increase the rate of oxidation. This is observed initially by TG as a relative increase in the rate of the weight gain from dry to wet atmospheres. However, after the initial fast parabolic growth, the constant linear evaporation of chromium containing species starts to influence the TG data, effectively decreasing the relative weight gain [34–36]. The fact that the rate of evaporation increases with increasing water vapor pressures, accordingly, counteracts the increased oxidation rate due to protons. During operation of a PCFC, water will be formed on the cathode, and the interconnect will thereby inevitably be exposed to high partial pressures of water in the oxidizing cathode gas atmosphere. In this respect it is beneficial with an outer layer of chromium manganese spinel that reduces the evaporation of chromium species [34]. To limit the evaporation further, metallic coatings of Co and Ce have been tested with promising results [37].

The oxidation study presented in this paper shows that Sandvik Sanergy HT is susceptible to accelerated oxidation at sufficiently high temperatures. Although this behavior only was observed at 1000 °C, it may also occur at lower temperatures by increasing the duration of oxidation [38–40]. By using the critical mass gain initiating accelerated oxidation at 1000 °C (~3.9 mg cm^{-2} after 300 h) and the assumption that the oxidation behavior remains the same at 800 °C, a first approximation of the time to reach accelerated oxidation far exceeds the expected life time of a fuel cell (>50,000 h).

As a consequence of the limited scale growth at 700 °C and the formation of oxides with inherent high electronic conductivity, the ASR of Sandvik Sanergy HT measured in this study proved to be low. The decreasing ASR indicates that the resistance due to the initially poor contact is much higher than the resistance induced by the growth of the oxide scale, and further that the improved electrical contact outweighs the negative influence of the increasing oxide thickness. The oxidation rate measured at this temperature was low, hence, the time of which the increased oxide scale thickness would lead to a significant increase in ASR could be long. One may argue that the recorded ASR in this study is influenced by the experimental setup, and that the oxide thickness may be reduced due to the Pt-electrode covering the sample surfaces. However, the interconnect will not be allowed to oxidize freely in a fuel cell assembly, but will operate in contact with other materials (e.g. anode and cathode). The variety of methods for determining ASR reported in literature calls for a standardized experimental setup for comparison reasons [17,41,42]. Since the expected operation temperature of a PCFC is 600–700 °C the low ASR presented in this study suggests that the Sandvik Sanergy HT may perform well during the operation of a PCFC.

At higher temperatures the oxidation rate is increased, hence a higher overall ASR would be expected despite that also the electrical conductivity of the semiconducting oxide is improved with increasing temperature (small polaron hopping). By assuming that the ASR is directly related to the thickness of the oxide, the resulting ASR can be calculated based on the parabolic rate constants, the density of the scale and its conductivity [43]. In a worst case scenario with Cr_2O_3 as the predominating oxide it would only take ~150 h of oxidation at 800 °C to form an oxide scale 1 μm thick, and reach the threshold ASR value of 10 mΩ cm^2. However, as shown in this study, the oxide scale also comprises Cr–Mn spinels that will result in a lower ASR, especially if the spinel phases also contain Fe [44]. Further improving the oxidation resistance and/or the electrical conductivity of the oxide may be accomplished by means of surface coatings.

From Fig. 1 it is obvious that the thermal expansion behavior of the alloy at high temperatures deviates from the candidate electrolyte, $LaNbO_4$. The discrepancy between these two materials in the high temperature region (>510 °C) will necessarily induce mechanical stresses in a fuel cell configuration, particularly critical during thermal cycling. Whether the stresses are in the range that can eventually lead to a mechanical breakdown of the fuel cell

stack is difficult to establish without a complete stress test of the fuel cell.

5. Conclusions

Several high temperature properties of Sandvik Sanergy HT were investigated under oxidizing (cathode) fuel cell operating conditions to establish its potential as a metallic interconnect for PCFCs based on $LaNbO_4$ electrolytes. The material holds a high oxidation resistance and forms oxides with relatively high electrical conductivity. However, coatings may be required to further improve the performance of the material for practical applications. Some concern was also raised regarding the deviation in thermal expansion between the mentioned interconnect material and the $LaNbO_4$ electrolyte. Sandvik Sanergy HT undergoes accelerated oxidation at 1000 °C, but this not expected to occur at lower temperatures within the expected life time of a fuel cell. Overall Sandvik Sanergy HT is considered a promising candidate as a metallic interconnect for $LaNbO_4$ based PCFCs.

Acknowledgement

This work is supported by the RENERGI project 185322 “Stack Technology for Ceramic Proton Conductors (StackPro)” of the Research Council of Norway.

References

[1] R. Haugsrud, T. Norby, Solid State Ionics 177 (2006) 1129–1135.
[2] K.D. Kreuer, Annu. Rev. Mater. Res. 33 (2003) 333–359.
[3] A. Magraso, M.L. Fontaine, Y. Larring, R. Bredesen, G.E. Syvertsen, H.L. Lein, T. Grande, M. Huse, R. Strandbakke, R. Haugsrud, T. Norby, Fuel Cells 11 (2011) 17–25.
[4] J.W. Fergus, Mater. Sci. Eng. A 397 (2005) 271–283.
[5] P. Kofstad, R. Bredesen, Solid State Ionics 52 (1992).
[6] W.J. Quadakkers, J. Piron-Abellan, V. Shemet, L. Singheiser, Mater. High Temp. 20 (2003) 115–127.
[7] L. Mikkelsen, K. Neufeld, P.V. Hendriksen, ECS Trans. 25 (2009) 1429–1436.
[8] H.T. Sanergy, Material Data Sheet, Sandvik Materials Technology, 2009.
[9] L. Jian, C.M. Wayman, J. Am. Ceram. Soc. 80 (1997) 803–806.
[10] T. Mokkelbost, H.L. Lein, P.E. Vullum, R. Holmestad, T. Grande, M.-A. Einarsrud, Ceram. Int. 35 (2009) 2877–2883.
[11] A.M. Huntz, A. Reckmann, C. Haut, C. Sévérac, M. Herbst, F.C.T. Resende, A.C.S. Sabioni, Mater. Sci. Eng. A 447 (2007) 266–276.
[12] M. Palcut, L. Mikkelsen, K. Neufeld, M. Chen, R. Knibbe, P.V. Hendriksen, Corros. Sci. 52 (2010) 3309–3320.
[13] T. Brylewski, J. Dąbek, K. Przybylski, J. Therm. Anal. Calorim. 77 (2004) 207–216.
[14] M.d.F. Salgado, A.C.S. Sabioni, A.-M. Huntz, E.H. Rossi, Mater. Res. (Sao Carlos Braz.) 11 (2008) 227–232.
[15] I. Antepara, I. Villarreal, L.M. Rodríguez-Martínez, N. Lecanda, U. Castro, A. Laresgoiti, J. Power Sources 151 (2005) 103–107.
[16] S. Fontana, S. Chevalier, G. Caboche, J. Power Sources 193 (2009) 136–145.
[17] S. Fontana, R. Amendola, S. Chevalier, P. Piccardo, G. Caboche, M. Viviani, R. Molins, M. Sennour, J. Power Sources 171 (2007) 652–662.
[18] C.J. Fu, K.N. Sun, N.Q. Zhang, X.B. Chen, D.R. Zhou, Thin Solid Films 516 (2008) 1857–1863.
[19] T. Brylewski, T. Maruyama, M. Nanko, K. Przybylski, J. Therm. Anal. Calorim. 55 (1999) 681–690.
[20] M.G.C. Cox, B. McEnaney, V.D. Scott, Philos. Mag. 26 (1972) 839–851.
[21] R.E. Lobnig, H.P. Schmidt, K. Hennesen, H.J. Grabke, Oxid. Met. 37 (1992) 81–93.
[22] A.C.S. Sabioni, A.M. Huntz, L.C. Borges, F. Jomard, Philos. Mag. 87 (2007) 1921–1937.
[23] R.K. Wild, Corros. Sci. 17 (1977) 87–104.
[24] P. Kofstad, High Temperature Corrosion, 1 ed., Elsevier Applied Science, 1988.
[25] W.C. Hagel, J. Am. Ceram. Soc. 48 (1965) 70–75.
[26] W.C. Hagel, A.U. Seybolt, J. Electrochem. Soc. 108 (1961) 1146–1152.
[27] D.J. Young, Mater. Sci. Forum 595–598 (2008) 1189–1197.
[28] P. Kofstad, Oxid. Met. 44 (1995) 3–27.
[29] T. Norby, Adv. Ceram. 23 (1987) 107–123.
[30] T. Norby, J. Phys. IV 3 (1993) 99–106.
[31] Y. Zhenguo, M.S. Walker, P. Singh, J.W. Stevenson, T. Norby, J. Electrochem. Soc. 151 (2004) B669–B678.
[32] B. Tveten, G. Hultquist, T. Norby, Oxid. Met. 51 (1999) 221–233.
[33] A. Holt, P. Kofstad, Solid State Ionics 69 (1994) 127–136.
[34] G.R. Holcomb, D.E. Alman, Scripta Mater. 54 (2006) 1821–1825.
[35] D.D.K. Hilpert, M. Miller, D.H. Peck, R. Weiss, J. Electrochem. Soc. 143 (1996).
[36] H. Asteman, K. Segerdahl, J.-E. Svensson, L.-G. Johansson, Mater. Sci. Forum 5 (2001) 369–372.
[37] J. Froitzheim, J.E. Svensson, ECS Trans. 35 (2011) 2503–2508.
[38] I. Gurrappa, S. Weinbruch, D. Naumenko, W.J. Quadakkers, Mater. Corros. 51 (2000) 224–235.
[39] P. Huczkowski, V. Shemet, J. Piron-Abellan, L. Singheiser, W.J. Quadakkers, N. Christiansen, Mater. Corros. 55 (2004) 825–830.
[40] W.J. Quadakkers, K. Bongartz, Mater. Corros. 45 (1994) 232–241.
[41] X. Xin, S. Wang, Q. Zhu, Y. Xu, T. Wen, Electrochem. Commun. 12 (2010) 40–43.
[42] P. Piccardo, P. Gannon, S. Chevalier, M. Viviani, A. Barbucci, G. Caboche, R. Amendola, S. Fontana, Surf. Coat. Technol. 202 (2007) 1221–1225.
[43] P.Y. Hou, K. Huang, W.T. Bakker, Proc. Electrochem. Soc. 99-19 (1999) 737–748.
[44] N. Sakai, T. Horita, Y.P. Xiong, K. Yamaji, H. Kishimoto, M.E. Brito, H. Yokokawa, T. Maruyama, Solid State Ionics 176 (2005) 681–686.